

# PCCP

Accepted Manuscript



This is an *Accepted Manuscript*, which has been through the Royal Society of Chemistry peer review process and has been accepted for publication.

*Accepted Manuscripts* are published online shortly after acceptance, before technical editing, formatting and proof reading. Using this free service, authors can make their results available to the community, in citable form, before we publish the edited article. We will replace this *Accepted Manuscript* with the edited and formatted *Advance Article* as soon as it is available.

You can find more information about *Accepted Manuscripts* in the [Information for Authors](#).

Please note that technical editing may introduce minor changes to the text and/or graphics, which may alter content. The journal's standard [Terms & Conditions](#) and the [Ethical guidelines](#) still apply. In no event shall the Royal Society of Chemistry be held responsible for any errors or omissions in this *Accepted Manuscript* or any consequences arising from the use of any information it contains.

# Molecular Dynamic Study of a CNT/Buckyballs-enabled Energy Absorption System

Heng Chen<sup>ab</sup>, Liuyang Zhang<sup>b</sup>, Matthew Becton<sup>b</sup>, Hong Nie<sup>a</sup>,  
Jinbao Chen<sup>a</sup>, and Xianqiao Wang<sup>b</sup>

<sup>a</sup> College of Aerospace Engineering, Nanjing University of Aeronautics and Astronautics,  
Nanjing, Jiangsu 210016 China

<sup>b</sup> College of Engineering, University of Georgia, Athens, GA 30602 USA

## Abstract

An energy absorption system (EAS) composed of a carbon nanotube (CNT) with nested buckyballs is put forward for energy dissipation during the impact owing to the outstanding mechanical properties of both CNTs and buckyballs. Here we implement a series of molecular dynamics (MD) simulations to investigate the energy absorption capability of several different EASs based on a variety of design parameters. For example, effects of impact energy, effects of the number of nested buckyballs, and effects of the size of buckyballs are analyzed to optimize the energy absorption capability of the EASs by tuning the relevant design parameters. Simulation results indicate that energy absorption capability of the EAS is closely associated with the deformation characteristics of the confined buckyballs. Low impact energy leads to recoverable deformation of buckyballs and the dissipated energy is mainly converted to thermal energy. However, high impact energy yields non-recoverable deformation of buckyballs and thus the energy dissipation is dominated by the strain energy of the EAS. Simulation results also reveal that there exists an optimal value of the number of buckyballs for an EAS under certain impact energy. Larger buckyballs are able to deform to a larger degree yet also need less impact energy to induce the plastic deformation, therefore performing better overall energy absorption ability. Overall, the EAS in this study show a remarkably high energy absorption density 2 kJ/g

which provides a promising candidate for mitigating impact energy and shed light on the research of buckyball-filled CNTs for other applications.

**Keywords:** Energy absorption, Impact, Carbon Nanotube, Buckyball, Molecular Dynamics

## 1. Introduction

Energy absorption materials or structures have long been a hot research topic in engineering<sup>1,2</sup>. Their primary purpose is to protect critical structures or human in a crash event by mitigating the impact energy and loading magnitude substantially. Traditionally, the most widespread used material for energy mitigation is metal for its structural failure and plastic deformation<sup>3-5</sup>. Foam-filled columns<sup>6-11</sup> and sandwich structures<sup>12-17</sup> also show excellent performance in mitigating energy propagation due to their buckling mechanism. Another conventional form for energy absorption is internal damping by polymer composites<sup>18-22</sup>. However, these materials with an ultimate energy absorption density not exceeding 10 J/g cannot satisfy the ever-increasing requirement for lighter weight, smaller volume, and higher energy dissipation efficiency<sup>23</sup>.

Recent results reveal that structured nanomaterials are superb contenders for energy mitigation, which can be attributed to their splendid mechanical properties including enhanced surface-to-volume, strength-to-weight, and stiffness-to-weight ratios, etc.<sup>23-27</sup>. For examples, polymer-based nanocomposite is superior to conventional polymer composite mainly because of its enhanced toughness<sup>27</sup>. A nanoporous energy absorption system consisting of non-wetting liquid and nanoporous particles possesses energy absorption density about 15 J/g larger than that of conventional systems<sup>23, 27-30</sup>. CNT-based nanocomposites also have properties which are conducive to energy absorption<sup>31-36</sup>. Carbon fiber reinforced plastic laminate, which is usually brittle, demonstrates good impact behavior and absorbs a certain amount of impact energy when

applied with a coating of CNT/epoxy nanocomposites<sup>31</sup>. Furthermore, the increasing understanding of the fullerene family<sup>37-39</sup> assists in designing novel energy absorption systems with much higher energy absorption density than those currently available. As a member of the fullerene family, carbon nanotubes (CNTs) have demonstrated an excellent energy absorption capability in foams and three-dimensional sponge-array architectures<sup>40-42</sup> due to their unprecedented mechanical properties. Both experimental and computational results revealed that CNTs have extremely large surface area, high strength and stiffness, and extraordinarily light weight compared to traditional materials (Young's modulus of over 1 TPa, tensile strength of 200 GPa, shear modulus of about 1 GPa, bulk modulus of 462-546 GPa and bending strength of around 14.2 GPa)<sup>43-45</sup>. Buckyballs, another important fullerene, are also verified to have intriguing mechanical properties (bulk modulus of 903 GPa for an individual C<sub>60</sub><sup>46</sup>) but unique deformation characteristics<sup>47, 48</sup>. Smith and Man<sup>49, 50</sup> verified that C<sub>60</sub> fullerene remained intact in low-energy collisions with graphite surfaces yet had a large deformation in higher-energy collisions and this deformation was observed to rebound to the original configuration. Zhang and Becton<sup>51, 52</sup> also investigated the phenomenon of buckyballs-graphene collisions and found that the buckyball bounced back under low impact energy yet stucked to the graphene and even penetrated through a single-layer graphene at high impact energy with recoverable deformation. Xu et al.<sup>53</sup> found that for smaller buckyballs, impact energy was mainly converted to thermal energy, whereas larger buckyballs tended to have non-recoverable deformation and thus strain energy was responsible for a majority of the energy dissipation, which was more beneficial for energy absorption systems.

In addition, some experimental results reveals that core-filled CNTs, such as C<sub>60</sub>- Fe- and ZnS-filled CNTs, have much more enhanced mechanical property than empty CNTs<sup>54-58</sup>. However,

few studies have focused on taking benefits of structure strength from CNT and energy absorption capability from buckyballs. Therefore, this paper puts forward an energy absorption system made of buckyball-filled CNT. The major functions of CNT are structural support for carrying the mechanical load, maintaining the structural integrity, confining the buckyballs and reducing the contact force. Molecular dynamics (MD) simulations are carried out to investigate the impact performance and energy absorption capability of this EAS. To better understand the energy absorption characteristics, the effects of impact energy, number of nested buckyballs, and buckyball size on energy absorption performance are analyzed in addition to the evolution of the deformation process during the impact procedure. This study can provide in-depth understanding of the impact properties of buckyball-filled CNTs and offer a promising candidate for energy mitigation.

## 2. Model and computational Methods

A single-walled carbon nanotube (SWCNT),  $C_{180}$  buckyball, and  $C_{720}$  buckyball<sup>59-61</sup> are selected to construct the energy absorption system (EAS) of interest. Figure 1 depicts the computational model, in which the EAS is supported by a lower fixed rigid plate (receiver), and experiences impact induced by the upper rigid plate (impactor) with the mass of 5.20 ng and a set of initial impact velocities. According to the interlayer spacing 3.4 Å of multi-walled carbon nanotube and diameters of  $C_{180}$  and  $C_{720}$  buckyballs, the diameter of the SWCNT in this study is chosen to be 31.8 Å<sup>62</sup>. For the EAS with five  $C_{720}$  fullerenes (5- $C_{720}$  EAS), the distance  $L_0$  between the center of mass of two adjacent balls is set to be 28.4 Å and the length  $L$  of the SCNT is 142 Å. For the purpose of simplification in terms of interatomic potentials, here we assume both the impactor and the consisting of carbon atoms with the same length of SWCNT and the width equal to half of the perimeter of the SWCNT. Therefore, in the whole system only carbon-

carbon atomic interactions exist. In order to investigate the effects of the number of buckyballs on energy absorption performance, a set of different numbers of C<sub>720</sub> buckyballs (2, 3, 4, and 5) are used to fill the SWCNT. To demonstrate the effect of buckyball size, twenty C<sub>180</sub> buckyballs are utilized to construct a 20-C<sub>180</sub> EAS which has the same mass of the 5-C<sub>720</sub> EAS.

In this work, MD simulations are carried out based on the open source platform LAMMPS (Large-scale Atomic/Molecular Massively Parallel Simulator)<sup>63</sup>. During the initial equilibrium process, a canonical ensemble (NVT) is applied to drive the temperature of the system to the desired 300 K. Afterwards, a microcanonical ensemble (NVE) is adopted in order to maintain the total energy of the system. Therefore, the kinetic energy of the impactor is transferred and dissipated in the form of the potential and kinetic energy of the EAS. A pairwise 6-12 Lennard-Jones potential is added to account for buckyball-buckyball and buckyball-CNT interactions

$$E = 4\epsilon \left[ \left( \frac{\sigma}{r} \right)^{12} - \left( \frac{\sigma}{r} \right)^6 \right], \quad r < r_c \quad (1)$$

where  $\epsilon$  is the carbon-carbon potential well depth,  $\sigma$  is the critical distance where the carbon-carbon potential is zero,  $r$  is the distance between carbon atoms, and  $r_c$  is the cutoff. Here the values of parameters  $\epsilon$  and  $\sigma$  are 2.875 meV and 3.47 Å respectively<sup>64, 65</sup>. Furthermore, as an optimal choice for carbon and hydrogen systems, the adaptive intermolecular reactive empirical bond order (AIREBO) potential proposed by Stuart et al.<sup>66</sup> is utilized to illustrate the carbon-carbon interaction intra-buckyball and intra-CNT including three terms as follows:

$$E = \frac{1}{2} \sum_i \sum_{j \neq i} [E_{ij}^{REBO} + E_{ij}^{LJ} + \sum_{k \neq i, j} \sum_{l \neq i, j, k} E_{ijkl}^{TORSION}] \quad (2)$$

where  $E_{ij}^{REBO}$  means REBO (reactive empirical bond order) potential developed by Brenner et al.<sup>67</sup> and demonstrates carbon-carbon interactions between atom  $i$  and  $j$  ranged less than 2 Å.

The  $E_{ij}^{LJ}$  term, a similar form to the standard Lennard-Jones potential but excluding what the  $E_{ij}^{REBO}$  term includes, describes the longer-ranged pairwise interactions. Meanwhile a cutoff distance should be set so as to control the extension of interactions captured by the  $E_{ij}^{LJ}$  term. As a tradeoff of computational efficiency and accuracy, the cutoff distance is determined as 10.2 Å in the present work. Periodical boundary conditions are applied along the z-axis to prevent boundary effects and two standard 6-12 L-J walls are added to both sides of the SWCNT at  $x = \pm 26$  Å to restrict the SWCNT to drift excessively along the x axis but reserve enough space for deformation during the impact process.

### 3. Results and Discussions

#### 3.1 Effects of impact energy

To understand the effect of impact energy on energy absorption capability of EAS, different impact velocities varying from 20 m/s to 400 m/s are applied to the impactor so as to generate different impact energies (from 64.88 eV to 10.138 keV) based on the 5-C<sub>720</sub> EAS. All simulations demonstrate an important phenomenon wherein the deformation of both the SWCNT and the buckyballs exhibit different characteristics. For the SWCNT, during the impact process, a trapezoid deformation and an inverted-trapezoid deformation alternatively evolve in turn. When the impact energy is very low, the deformation of SWCNT is fully recoverable. For the high impact energy, although the SWCNT can't rebound to the original configuration absolutely, the non-recoverable deformation compared with buckyballs is negligible as demonstrated in Figure 2. For the buckyballs, small impact energy also generates recoverable deformation. As the impact energy increases, non-recoverable deformation emerges in buckyballs gradually. Then all the buckyballs have non-recoverable deformation, and the evolution processes of their

deformations of are similar for a single impact. Afterwards the extent of non-recoverable deformation becomes more and more violent until reaching a saturation state. The deformation of a buckyball can be illustrated to some extent by the radius of gyration (RoG) and asphericity value which are respectively expressed as:

$$R_g = \sqrt{\frac{1}{N} \sum_{i=1}^N (r_i - r_0)^2} \quad (3)$$

$$b = \lambda_z^2 - \frac{1}{2}(\lambda_x^2 + \lambda_y^2) \quad (4)$$

where  $N$  is the number of carbon atoms in a buckyball,  $r_i$  and  $r_0$  are the positions of the  $i$ th atom and the mass center of the buckyball respectively,  $\lambda_x$ ,  $\lambda_y$  and  $\lambda_z$  are principle moments of the gyration tensor. Figure 3 shows the evolution of the RoG and asphericity of a buckyball under two different impact energies 1.038 keV and 4.152 keV, representing two typical deformation mechanisms - fully recoverable and non-recoverable – respectively. Before the displacement of the impactor reaches 10 Å, the RoG of the buckyball hardly changes and little deformation of the buckyball appears, as interactions between the impactor and buckyballs are very small. Before the impactor starts to rebound in the low impact energy case, the evolution pathways of the RoG for both cases almost coincide with each other since the impactors can reach the same distance for both cases. From the observation of the cross-section of crumpled buckyballs, it is noticed that a biconcave shape appears firstly, tends to become flatter as the impact continues, and then develops to a W-shape, during which the radius of gyration of this buckyball keeps reducing. However, when rebound happens in the low energy case the evolution pathways of the RoG in both cases deviate from each other, and the final morphology of the buckyball depends on the initial impact energy. For the case of low impact energy, the deformation of the buckyball is reversible, and the evolution of the RoG reverses the pathway back to its original status. But for

the case of high impact energy, the impactor continues to compress the EAS until the buckyballs become a “disk”, which results in a quick linear increase of the radius of gyration of the buckyball till the maximum value quickly. As the impactor starts to rebound, the RoG of the buckyball experience a quick drop to the value of 11.3 Å, and the morphology of the buckyball evolves to an intriguing V-shape. The shape “V” then becomes unsymmetrical, resulting in the slight rise of the RoG of the buckyball. In what follows, the morphology as well as the RoG of the buckyball reaches to a stable status, even though the deformation of the SWCNT continues to reverse until the impactor completely detaches from the SWCNT (see in Figure 2 (h) and (i)).

Similar to the RoG, before the impactor starts to rebound in the low impact energy case, the evolution pathways of the asphericity for both cases almost coincide with each other since the impactors can reach the same distance for both cases. The difference is that the asphericity value keeps increasing generally with slight fluctuations during the entire compression process. As the impactor starts to rebound, the asphericity experiences a short fluctuation and then reaches the peak at a “V” shape. Afterwards it keeps decreasing until the detachment between the impactor and system happens. It is found that the asphericity during the rebounding process is always larger than that during the compression process while at the same displacement, due to the unrecoverable deformation of the buckyball.

Owing to the large deformation of the EAS, it is obvious that contact force between the impactor and receiver can be attenuated to a great extent compared with a rigid impact system<sup>68</sup>.

Following the work-kinetic energy relationship, we can have

$$\int \mathbf{F} \cdot d\mathbf{y} = \Delta E_k \quad (4)$$

where  $F$  is the contact force induced on the impactor,  $y$  is the displacement of the impactor, and  $\Delta E_k$  is the difference value between the initial impact energy ( $E_{impactor}$ ) and the remaining kinetic energy ( $E'_{impactor}$ ) after detachment of the impactor from the receiver. As depicted in Figure 4, the contact force shows a slow increase since the buckyball experiences a linear deformation at its early stage of impact and possesses enough room to sustain the deformation. Then it follows a short period of decrease in which the morphology of the buckyball experiences a transition change from a sphere to a biconcave structure leading to the reduction of interactions among SWCNT, buckyballs and the impactor. After the short decrease, the contact force once again increases accompanied with a slight increase of the slope till the formation of a mature biconcave. Once the W-shaped cross-section of the buckyball appears, the rise of the contact force becomes quicker since the deformation of the buckyball is close to its limitation and it becomes more and more difficult to densify the buckyball. When the compression ends, the contact force arrives at the peak value. During the rebound process, the contact force drops rapidly to a value close to zero and then approaches zero steadily because the unrecoverable deformation of buckyballs increases the interaction distance and further decline the interaction between impactor and the remaining part of system. The area surrounded by the closed curve in the contact force-displacement plot indicates the work done by the contact force which has been confirmed to be equal to the energy absorbed by the EAS. With the growth of impact energy, the impactor deforms the EAS further accompanied with an increase in the maximum contact force and an increase in the energy absorption by the EAS.

In order to quantify the relationship between the energy absorption efficiency of the EAS and impact energy, here we define the energy absorption efficiency  $\eta$  as  $\Delta E_{impactor}/E_{impactor}$ . According to the principle of conservation of energy, it can be expected that the energy absorbed

by the EAS is partially converted to the increased kinetic energy of atoms in the EAS ( $\Delta E_{kinetic}$ ) and the remaining part is transformed to its extra potential energy ( $\Delta E_{potential}$ ). Since the kinetic energy of all the atoms ( $E_{kinetic}$ ), the center-of-mass kinetic energy of the EAS ( $E_{m\_kinetic}$ ) and the thermal energy ( $E_{thermal}$ ) can be respectively expressed as  $E_{kinetic} = \sum_{i=1}^N \frac{1}{2} m_i v_i^2$ ,  $E_{m\_kinetic} = \frac{1}{2} M \bar{v}^2$  and  $E_{thermal} = \sum_{i=1}^N \frac{1}{2} m_i (v_i - \bar{v})^2$  where  $m_i$  is the mass of the  $i$ -th atom,  $v_i$  is the velocity of the  $i$ -th atom,  $M$  is the mass of the EAS and  $\bar{v}$  is the center-of-mass velocity of the EAS, we can get their relationship as follows:

$$E_{kinetic} = E_{m\_kinetic} + E_{thermal} \quad (5)$$

Figure 5 describes the evolution process of the two parts and the temperature of the EAS under impact energy 4.152 keV, which indicates that the major part of  $\Delta E_{kinetic}$  accounts for the excessive thermal energy causing the increase of the temperature while the rest of it is responsible for the moderate movement of buckyballs and SWCNT. The increment of the potential energy  $\Delta E_{potential}$  is mainly comprised of the strain energy of EAS caused by deformation while the rest of it is attributed to the relative motion between fullerenes. To better determine the dominating factor of the energy absorption and identify the roles  $\Delta E_{kinetic}$  and  $\Delta E_{potential}$  play during the impact process, we classify the impact behavior into two phases as shown in Figure 6. In phase I, it can be observed that most of the absorbed energy during the impact is transferred to the increase of the kinetic energy of the EAS indicating that the absorbed kinetic energy plays a dominating role in energy absorption in phase I. For detail, energy absorption rate rises sharply from 15.49% to 40.37% at point A ( $E_{impactor} = 0.406$  keV) as the impact energy grows. However, after reaching the relative peak value, the rate decreases to 28.19% at point B ( $E_{impactor} = 1.622$  keV). Meanwhile, the difference between the absorbed kinetic

energy and potential energy gradually decreases and is almost zero at point B. Point A where both the absorbed potential and kinetic energy by the EAS reaches a relative peak value is considered to be the point of the best energy absorption in phase I. The explanation of the characteristics in phase I can be elaborated as follows: the deformation of the buckyballs in this stage is recoverable after the impactor detaches from the EAS and thus the variation of the potential energy of the system is relative small. Meanwhile, the constraint placed on the positions of fullerenes by the L-J walls poses an obstacle for the EAS to dissipate more energy from the impact via the increase of the kinetic energy of fullerenes. With respect to phase II, the energy absorption rate rises again due to the rapid increase of the absorbed potential energy and the slow increase of the absorbed kinetic energy of EAS after point B. This is because the non-recoverable (plastic) deformation of a number of buckyballs appears gradually and thus absorbs the impact energy in the form of the increased strain energy. It is interesting to point out that all buckyballs exhibit non-recoverable deformation after point C ( $E_{impactor} = 2.741$  keV) where the energy absorption rate is similar to that at point A yet with different proportions of energy transformation. At point D ( $E_{impactor} = 4.688$  keV), the energy absorption rate achieves the maximum value (56.93%) and the difference between the two converted energy also reaches the peak, indicating that the absorbed energy due to the plastic deformation of buckyballs reaches to its maximum value and the absorbed potential energy plays the dominating role in this stage. Therefore, after point D the energy absorption efficiency keeps reducing since the EAS reaches its limiting energy absorption capability. Figure 6 also reveals that as the impact energy increases the maximum contact force induced on the impactor keeps rising and the trend goes sharper at lower impact energies while lessened at higher impact energies.

### 3.2 Effects of number of buckyballs

To better understand the effects of the number of buckyballs, comparisons of the CNT/buckyballs system and pure CNT are discussed in terms of mechanical behavior and energy absorption capability. Lateral compression is performed for the mechanical behavior. The relationship of stress and strain for both systems is depicted in Figure 7. In the early stage of stress-strain curve, the lateral compression Young's modulus is estimated 5GPa for CNT/buckyballs system based on the linear elastic theory. It is obvious that, compared to the pure CNT, the compressive capability of CNT/buckyballs system is enhanced to a great extent. There also exist a few big peaks in the stress-strain curve of the CNT/buckyballs system, which corresponds to the morphological evolution of  $C_{720}$  (as the insertions in Figure 7). For comparison of energy absorption capability, both CNT/buckyballs system and pure CNT are applied to be impacted with impact energy 4.15 keV. Then they are further compared with pure buckyballs system which is proved to have favorable energy absorption capability in the previous work<sup>69</sup>. The comparison results are exhibited in Table 1. It can be noticed that the energy absorption efficiency of the single CNT is low and the contact force is much larger than that of the other two systems. This can be explained that the CNT is very flexible to deform in the lateral direction and therefore prone to become flatted during the impaction but most of its deformation is recoverable after the impactor detaches from it, which can be inferred from the contact force-displacement curve during the loading and unloading process in Figure 8. The comparison results also reveal that buckyballs only system has energy absorption efficiency 15.02% higher than the CNT/buckyballs system. The reason is that buckyballs in the buckyballs only system possess more severely unrecoverable deformation, which can be seen in the subplots of Figure 8. However, according to Table 1, the maximum contact force of the buckyballs only system is 49.25% larger than that of the CNT/Buckyballs system. Therefore, by taking into

account the energy absorption capability and maximum impact force together, the CNT/buckyballs system is considered to be a better EAS for impaction.

In order to investigate the effect of the number of buckyballs on the EAS energy absorption capability, here besides 5-C<sub>720</sub> EAS, 2-C<sub>720</sub>, 3-C<sub>720</sub> and 4-C<sub>720</sub> EASs are utilized to perform the impact test. According to the stress-strain relationships of the four EASs depicted in Figure 9, it can be inferred that the EAS with more buckyballs possesses larger stiffness, that is to say, more impact energy is required to deform the buckyballs. Thus an EAS with more C<sub>720</sub> balls needs more impact energy for the transition from the kinetic to potential dominated phase, which means for EASs with more C<sub>720</sub> balls, the impactor needs do more work to arrive at the same displacement. Therefore the EAS can store more energy according to the work-energy theorem, resulting in a better energy capacity. For the purpose of comparison, impact simulations of different EASs are based on the same series of impact energy per unit mass (IEUM, defined as  $E_{impactor}/m_{EAS}$ , where  $m_{EAS}$  is the mass of EAS) ranging from 0.04 kJ/g to 4.15 kJ/g on the systems. As has been discussed in Section 3.1, when IEUM is very low, the deformation of buckyballs is recoverable. Simulation results show that an EAS with more buckyballs needs a larger IEUM to produce the non-recoverable deformation in buckyballs. That is, as the IEUM increases, non-recoverable deformation first appears in 2-C<sub>720</sub> EAS, followed by 3-C<sub>720</sub> EAS and so on. The reason is probably due to that the buckyballs' mass comprises an increasing proportion in the total mass of the EAS. Figure 10 shows the energy absorption status with IEUMs of 1.30 kJ/g and 3.32 kJ/g respectively. In the case where the IEUM is 1.30 kJ/g, only 2-C<sub>720</sub> EAS has non-recoverable deformation and therefore it shows the largest energy absorption. For the rest of the EASs, the energy absorption increases slightly with the increase of the number of buckyballs. In the case with IEUM 3.32 kJ/g, all the buckyballs of different EASs

have non-recoverable deformations, and as a result the energy absorption improves with the increase of the number of buckyballs.

Furthermore, energy absorption per unit mass (EAUM) determined by  $\Delta E_{impactor}/m_{EAS}$  is investigated. According to Figure 11, for a certain EAS, EAUM grows with the increasing IEUM. When IEUM increases from a small value wherein only recoverable deformation of buckyballs happens, the maximum EAUM is acquired first by 2-C<sub>720</sub> EAS and then from 3-C<sub>720</sub> EAS to 5-C<sub>720</sub> EAS in order. It's obvious that there exists an optimal IEUM for an EAS to fulfill its energy absorption capability and this value becomes larger with more buckyballs. When the IEUM reaches 0.66 kJ/g, non-recoverable deformation occurs in 2-C<sub>720</sub> EAS and thus the corresponding EAUM becomes larger than those of the other EASs. As the growth of IEUM continues, more extreme deformation improves the energy absorption capability. Therefore, when non-recoverable deformation of 3-C<sub>720</sub> EAS occurs to a certain degree, its EAUM exceeds that of the 2-C<sub>720</sub> EAS. As seen in Figure 11, the maximum EAUM moves rightwards from IEUM = 0.66 kJ/g to IEUM = 2.66 kJ/g where 5-C<sub>720</sub> EAS obtains the optimal EAUM. As the impact energy increase, the deformation of the EAS reaches its limitation from the 2-C<sub>720</sub> EAS to the 5-C<sub>720</sub> EAS in order. Upon the impact with the same IEUM, the EAS show a lower EAUM than the others when it reaches the deformation limit first. However, after all EASs reach their deformation limit, an EAS with more buckyballs presents a larger EAUM.

To design a high-performance impactor receiver, beside the energy absorption per unit mass, the energy absorption efficiency, which also can be calculated from EAUM/IEUM, is another important criterion for evaluating the capability of energy absorption systems. Here we perform a series of simulations on the C<sub>720</sub> EASs with the IEUM from 1.30 kJ/g to 5.19 kJ/g such that the

non-recoverable deformation happens at least in one of the four  $C_{720}$  EAS. As Figure 12 shows, at  $IEUM = 1.30\text{kJ/g}$ , the energy absorption rate of 2- $C_{720}$  EAS is much larger than those of other EASs because only 2- $C_{720}$  EAS shows the non-recoverable deformation in the 2- $C_{720}$  buckyballs. The energy absorption rate of 3- $C_{720}$  EAS increases greatly with the IEUM from  $1.30\text{kJ/g}$  to  $1.87\text{kJ/g}$  but is still less than that of 2- $C_{720}$  EAS. It can be explained that the non-recoverable deformation just occurs in the 3- $C_{720}$  EAS but the 2- $C_{720}$  EAS evolves into a deeper buckling morphology. The highest energy absorption rates at  $IEUM = 2.54\text{kJ/g}$  and  $IEUM = 3.32\text{kJ/g}$  are obtained by the 4- $C_{720}$  EAS and 5- $C_{720}$  EAS respectively because of their significant non-recoverable deformations. With the increase of impact energy the energy absorption rate of the EAS decreases after the EAS achieves its deformation limit as we have discussed in Figure 13. EASs with fewer buckyballs arrive at the first peak more quickly and have a larger peak value of energy absorption percentage in phase I because there is more space in the SWCNT for buckyballs moving to absorb impact energy and transfer into the kinetic energy. Besides that, EASs with fewer buckyballs enter into phase II earlier due to the larger stiffness and then achieve the second peak faster as well, yet have a lower peak value. That is because buckyballs as the major energy dissipation part take a relative small proportion of the total mass in the EAS. Moreover, since the EAS with fewer buckyballs is easier to reach its deformation limit and then have less EAUM, it can be inferred that the energy absorption efficiency of EASs with fewer buckyballs gets steady more quickly and has a larger final rate. Consequently, it is essential to choose the appropriate number of buckyballs for an EAS to optimize its energy absorption performance.

### 3.3 Effects of ball size

Since the 5-C<sub>720</sub> EAS and 20-C<sub>180</sub> EAS have the same mass, the same impact energy means the same IEUM. According to Figure 9, it is also indicated that a tiny force is required to deform the 20-C<sub>180</sub> EAS when strain is less than 0.35. The reason is that at the beginning the buckyballs randomly arrange in the tube because of the equilibrium process and then position themselves almost in a plane since the impactor proceeds causing the CNT to become flatter (which can be seen in Figure 14 (a)-(b)). During this process, little deformation appears in C<sub>180</sub> balls. Hereafter the stiffness of 20-C<sub>180</sub> EAS becomes significantly large and soon surpasses that of 5-C<sub>720</sub> EAS. Impact velocities varying from 20 m/s to 200 m/s are given to the impactors of both two EASs. The simulation results show that upon impact with enough energy C<sub>180</sub> fullerenes in an EAS also exhibit non-recoverable deformation capability, although to a lesser extent than C<sub>720</sub>. Thus more storage energy in C<sub>180</sub> balls will be transferred back to the impactor during the rebound process, resulting in less energy absorption. For example, Figure 14 shows the deformation evolution of C<sub>180</sub> buckyballs during the impact process with an impact velocity of 160 m/s, which can be compared with the results in Figure 3. After the buckyballs position themselves in a plane, the deformation evolution, similar to that of C<sub>720</sub> buckyball but more simple, experiences biconcave, disk and biconvex shapes in order. As a result, the two EASs show the similar changing pattern of the energy absorption capability with the increase of impact energy irrespective of their own characteristics. As is shown in Figure 15, the energy absorption increases with the increase of impact velocity and the absorbed potential energy takes up the large portion of the absorbed total energy until the EAS reaches its deformation limit. At the initial stage, the increase of the energy absorption by EAS is gentle followed a quick increase when the non-recoverable deformation occurs in the EAS and towards a saturated status because of the deformation limit. What's different is that non-recoverable deformations of the 20-C<sub>180</sub> EAS and 5-C<sub>720</sub> EAS occur at

impact velocity at least 100 m/s and 120 respectively, which means that the  $C_{180}$ -EAS needs a higher impact energy for non-recoverable deformation because of the larger stiffness. At the instant of impact (with velocity 20 m/s  $v$  is the impact velocity) the energy absorption of the  $C_{180}$  EAS is much larger than that of  $C_{720}$  EAS. Because the impact energy is so low that it makes little influence on the  $C_{720}$  EAS but it is also able to flatten the SWCNT during the compression process and thus place the disordered buckyballs in a plane. Then when the impact velocity rises to 40 m/s, the energy absorption of the  $C_{720}$  EAS climbs fast, however, this impact energy has little further influence on the  $C_{180}$  EAS and thus the increase of the energy absorption is relatively small. Afterwards, the energy absorption of the  $C_{180}$  EAS also enters into an ascending stage following that of the  $C_{720}$  EAS, which is also reflected in Figure 16. Likewise, the  $C_{180}$  EAS experiences the similar phases I and II as we have discussed for the  $C_{720}$  EAS in Section 3.1. Compared with the  $C_{720}$  EAS, the transition for the  $C_{180}$  EAS happens at a high impact energy due to its larger stiffness. Since  $C_{180}$  can sustain a relative small deformation comparing with  $C_{720}$ , the  $C_{180}$  EAS absorbs less impact energy and leads to a smaller energy absorption percentage. In addition, the maximum contact force keeps rising with impact velocity from 20 m/s to 200 m/s for both the two EASs with a growing increment speed. The force exerting on the 20- $C_{180}$  EAS is higher than that on the 5- $C_{720}$  EAS for a variety of impact velocity. Generally, the 5- $C_{720}$  EAS possesses a better energy absorption performance than the 20- $C_{180}$  EAS, as it bestows a larger energy absorption rate but a smaller contact force.

#### 4. Conclusions

In this paper, an EAS consisting of a CNT and multiple nested buckyballs is put forward, and its energy absorption capability is investigated by performing a variety of MD simulations of

impacts with different design parameters including impact energy, the number of nested buckyballs and the size of buckyballs. Effects of these parameters are analysed in detail in order to pursue the best energy absorption capability of the EAS. Simulation results state that the deformation characteristics of the confined buckyballs play a crucial role in energy absorption capability of the EAS. At low impact energy buckyballs exhibit recoverable deformation and thus the energy absorption mainly owns to the increased thermal energy. At high impact energy buckyballs present non-recoverable deformation and the mitigated energy is mainly converted to the strain energy of the EAS, which is more beneficial for energy absorption ability. An EAS with larger stiffness needs more impact energy for the transition from the kinetic to potential dominated phase. The results also indicate that under certain impact energy the EAS can improve its energy absorption ability by tuning the number of the nested buckyballs. It is also found that larger buckyballs perform a better energy absorption capability because it generates larger deformation at the same impact energy and needs lower impact energy to yield plastic deformation. In addition, this EAS reveals an remarkably high energy absorption density as much as 2 kJ/g, which is especially available for weight-controlled products needing to possess the capability of crashworthiness such as an aircraft. Overall, although these researches are performed in silico, the results can provide a promising candidate from the computational viewpoint itself for impact protection and energy dissipation, and offer insights into the research of buckyball-filled CNTs in other fields.

For the future work, more endeavor should be devoted to expand the realm of the impact energy the EAS can sustain and further improve the energy absorption capability of the EAS, for examples, effects of the size of the SWCNT, comparison of the SWCNT and MWCNT (multi-walled carbon nanotube), and effects of the rolled layers of the MWCNT. Since a plenty of free

space between SWCNT and buckyballs exists, fluids or gases such as water and CO<sub>2</sub> can be placed to investigate their effects on energy absorption capability of EASs. Previous research have provided compelling evidences that <sup>28, 29, 70</sup> the change of solid-liquid or solid-gas interaction energy can be part of energy dissipation, therefore enhancing the system's energy absorption.

**Acknowledgements**

HC would like to appreciate the support from the Scholarship of Nanjing University of Aeronautics and Astronautics (China). LZ, MB, and XW would like to acknowledge support from the University of Georgia (UGA) Research Foundation. Calculations are performed at the UGA Advanced Computing Resource Centre.

**Author information**

Corresponding author: Xianqiao Wang

Email: xqwang@uga.edu.

Competing financial interests: The authors declare no competing financial interests.

## References

1. V. U. Unnikrishnan, G. U. Unnikrishnan, J. N. Reddy and F. Rostam-Abadi, *International Journal of Mechanics and Materials in Design*, 2013, 9, 181-189.
2. L. Sun, R. F. Gibson, F. Gordaninejad and J. Suhr, *Composites Science and Technology*, 2009, 69, 2392-2409.
3. N. Jones, *International Journal of Impact Engineering*, 1993, 13, 161-161.
4. S. R. Reid, *International Journal of Mechanical Sciences*, 1993, 35, 177-177.
5. S. Ramakrishna, *Materials & Design*, 1997, 18, 167-173.
6. R. A. Alia, Z. Guan, N. Jones and W. J. Cantwell, *Journal of Sandwich Structures & Materials*, 2015, 17, 74-94.
7. S. Shahbeyk, A. Vafai and N. Petrinic, *Thin-Walled Structures*, 2005, 43, 1818-1830.
8. S. L. Lopatnikov, B. A. Gama, M. J. Haque, C. Krauthauser, J. W. Gillespie, M. Guden and I. W. Hall, *Composite Structures*, 2003, 61, 61-71.
9. S. Gordon, R. Boukhili and N. Merah, *Journal of Sandwich Structures & Materials*, 2014, 16, 551-574.
10. M. Li, X. Cao and Y. Luo, *Iranian Polymer Journal*, 2014, 23, 775-781.
11. M. I. Thiyahuddin, Y. T. Gu, D. P. Thambiratnam and H. M. Thilakarathna, *International Journal of Impact Engineering*, 2014, 72, 26-39.
12. A. Kolopp, S. Rivallant and C. Bouvet, *International Journal of Impact Engineering*, 2013, 61, 24-35.
13. M. A. Mousa and N. Uddin, *Aci Materials Journal*, 2014, 111, 99-109.
14. S. Sachse, M. Poruri, F. Silva, S. Michalowski, K. Pielichowski and J. Njuguna, *Journal of Sandwich Structures & Materials*, 2014, 16, 173-194.
15. Y. O. Shen, F. J. Yang, W. J. Cantwell, S. Balawi and Y. Li, *Journal of Reinforced Plastics and Composites*, 2014, 33, 1148-1157.
16. P. Navarro, S. Marguet, J. F. Ferrero, J. J. Barrau and S. Lemaire, *Mechanics of Advanced Materials and Structures*, 2012, 19, 523-529.
17. S. K. Garcia-Castillo, B. L. Buitrago and E. Barbero, *Polymer Composites*, 2011, 32, 290-296.
18. A. Argento, W. Kim, E. C. Lee, A. M. Harris and D. F. Mielewski, *Polymer Composites*, 2011, 32, 1423-1429.
19. J. Feuchtwanger, M. L. Richard, Y. J. Tang, A. E. Berkowitz, R. C. O'Handley and S. M. Allen, *Journal of Applied Physics*, 2005, 97.
20. G. C. Jacob, J. M. Starbuck, S. Simunovic and J. F. Fellers, *Polymer Composites*, 2003, 24, 706-715.
21. Y. Liu and X.-I. Gong, *Transactions of Nonferrous Metals Society of China*, 2006, 16, S439-S443.
22. M. Mahendran, J. Feuchtwanger, R. Techapiesanchaorenkij, D. Bono and R. C. O'Handley, *Journal of Magnetism and Magnetic Materials*, 2011, 323, 1098-1100.
23. Q. Zhang, E. Uchaker, S. L. Candelaria and G. Cao, *Chemical Society Reviews*, 2013, 42, 3127-3171.
24. H. T. Beyene, V. S. K. Chakravadhanula, C. Hanisch, M. Elbahri, T. Strunskus, V. Zaporajtchenko, L. Kienle and F. Faupel, *Journal of Materials Science*, 2010, 45, 5865-5871.
25. WO2014139028-A1.
26. H. T. Beyene, V. S. K. Chakravadhanula, C. Hanisch, T. Strunskus, V. Zaporajtchenko, M. Elbahri and F. Faupel, *Plasmonics*, 2012, 7, 107-114.
27. J. C. Viana, *Plastics Rubber and Composites*, 2006, 35, 260-267.
28. A. K. Al-Qananwah, J. Koplik and Y. Andreopoulos, *Physics of Fluids*, 2013, 25, 076102.
29. G. Cao, *The Journal of Physical Chemistry C*, 2012, 116, 8278-8286.

30. F. B. Surani, X. Kong, D. B. Panchal and Y. Qiao, *Applied Physics Letters*, 2005, 87, 163111.
31. D. Weidt, L. Figiel and M. Buggy, *International Conference on Structural Nano Composites (Nanostruc 2012)*, 2012, 40.
32. Z. Antar, J.-F. Feller and G. Vignaud, *Polymers for Advanced Technologies*, 2013, 24, 638-645.
33. Q. Chen, W. Wu, Y. Zhao, M. Xi, T. Xu and H. Fong, *Composites Part B-Engineering*, 2014, 58, 43-53.
34. X. Wang, X. Wang and L. Hu, *Asian Journal of Chemistry*, 2013, 25, 5798-5800.
35. K. Yu, Y. Liu and J. Leng, *Rsc Advances*, 2014, 4, 2961-2968.
36. X. Zhou, L. Shen, L. Li, S. Zhou, T. Huang, C. Hu, W. Pan, X. Jing, J. Sun, L. Gao and Q. Huang, *Journal of the European Ceramic Society*, 2013, 33, 2119-2126.
37. E. I. Bagrii and E. N. Karaulova, *Petroleum Chemistry*, 2001, 41, 295-313.
38. N. F. Gol'dshleger and A. P. Moravskii, *Petroleum Chemistry*, 2000, 40, 365-377.
39. S. V. Kozyrev and V. V. Rotkin, *Semiconductors*, 1993, 27, 777-791.
40. L. Lattanzi, L. De Nardo, J. R. Raney and C. Daraio, *Advanced Engineering Materials*, 2014, 16, 1026-1031.
41. X. Gui, Z. Zeng, Y. Zhu, H. Li, Z. Lin, Q. Gan, R. Xiang, A. Cao and Z. Tang, *Advanced Materials*, 2014, 26, 1248-1253.
42. L. Q. Liu, W. J. Ma and Z. Zhang, *Small*, 2011, 7, 1504-1520.
43. C. M. Wang, Y. Y. Zhang, Y. Xiang and J. N. Reddy, *Applied Mechanics Reviews*, 2010, 63.
44. E. T. Thostenson, Z. F. Ren and T. W. Chou, *Composites Science and Technology*, 2001, 61, 1899-1912.
45. M. R. Delfani, H. M. Shodja and F. Ojaghnezhad, *Philosophical Magazine*, 2013, 93, 2057-2088.
46. R. S. Ruoff and A. L. Ruoff, *Applied physics letters*, 1991, 59, 1553-1555.
47. N. Kaur, S. Gupta, K. Dharamvir and V. K. Jindal, *Behaviour of a bucky-ball under extreme internal and external pressures*, 2009.
48. A. V. Dyskin, Y. Estrin, A. J. Kanel-Belov and E. Pasternak, *Physics Letters A*, 2003, 319, 373-378.
49. Z. Man, Z. Pan and Y. Ho, *Physics Letters A*, 1995, 209, 53-56.
50. R. Smith and R. P. Webb, *Proceedings of the Royal Society of London. Series A: Mathematical and Physical Sciences*, 1993, 441, 495-499.
51. Z. Zhang, X. Wang and J. Li, *International Journal of Smart and Nano Materials*, 2012, 3, 14-22.
52. M. Becton, L. Zhang and X. Wang, *Journal of Nanomechanics and Micromechanics*, 2014, 4.
53. J. Xu, Y. Sun, B. Wang, Y. Li, Y. Xiang and X. Chen, *Mechanics Research Communications*, 2013, 49, 8-12.
54. P. M. Costa, P. B. Cachim, U. K. Gautam, Y. Bando and D. Golberg, *Nanotechnology*, 2009, 20, 405707.
55. W. Abramowicz and T. Wierzbicki, *International Journal of Mechanical Sciences*, 1988, 30, 263-271.
56. P. M. Costa, U. K. Gautam, M. Wang, Y. Bando and D. Golberg, *Carbon*, 2009, 47, 541-544.
57. F. Wolny, U. Weissker, T. Mühl, A. Leonhardt, S. Menzel, A. Winkler and B. Büchner, *Journal of Applied Physics*, 2008, 104, 064908.
58. A. O. Monteiro, P. B. Cachim and P. Costa, *Diam. Relat. Mat.*, 2014, 44, 11-25.
59. D. M. Anjos, A. I. Kolesnikov, Z. Wu, Y. Cai, M. Neurock, G. M. Brown and S. H. Overbury, *Carbon*, 2013, 52, 150-157.
60. L. Xie, Y. Luo, D. Lin, W. Xi, X. Yang and G. Wei, *Nanoscale*, 2014, 6, 9752-9762.
61. J. Xu, Y. Li, Y. Xiang and X. Chen, *Plos One*, 2013, 8.
62. O. V. Kharissova and B. I. Kharisov, *Rsc Advances*, 2014, 4, 30807-30815.
63. S. Plimpton, *Journal of Computational Physics*, 1995, 117, 1-19.
64. L. Girifalco and M. Hodak, *Physical Review B*, 2002, 65, 125404.

65. R. Saito, R. Matsuo, T. Kimura, G. Dresselhaus and M. S. Dresselhaus, *Chemical Physics Letters*, 2001, 348, 187-193.
66. S. J. Stuart, A. B. Tutein and J. A. Harrison, *Journal of Chemical Physics*, 2000, 112, 6472-6486.
67. D. W. Brenner, O. A. Shenderova, J. A. Harrison, S. J. Stuart, B. Ni and S. B. Sinnott, *Journal of Physics-Condensed Matter*, 2002, 14, 783-802.
68. H. Ruan, Z. Gao and T. Yu, *International journal of mechanical sciences*, 2006, 48, 117-133.
69. J. Xu, Y. Li, Y. Xiang and X. Chen, *Nanoscale Research Letters*, 2013, 8, 1-10.
70. H. Liu and G. Cao, *The Journal of Physical Chemistry C*, 2013, 117, 4245-4252.

**Table 1** Comparisons of the three energy absorption systems

$E_{\text{impactor}} = 4.15\text{keV}$	CNT/Buckyballs	Buckyballs	CNT
Energy absorption efficiency	56.34%	64.8%	9.79%
Maximum contact force ( $\mu\text{N}$ )	1.734	2.588	6.91

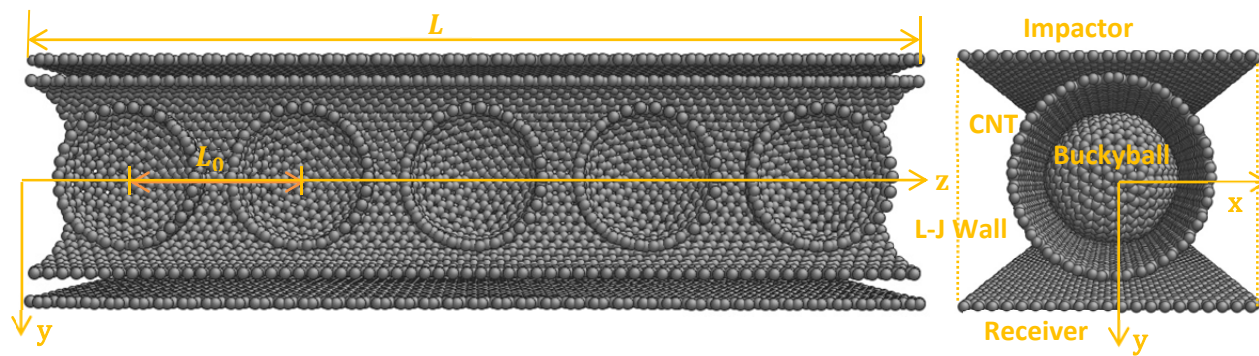


**Figure 1:** Computational cell based on 5-C<sub>720</sub> EAS and illustration of the coordinate system.

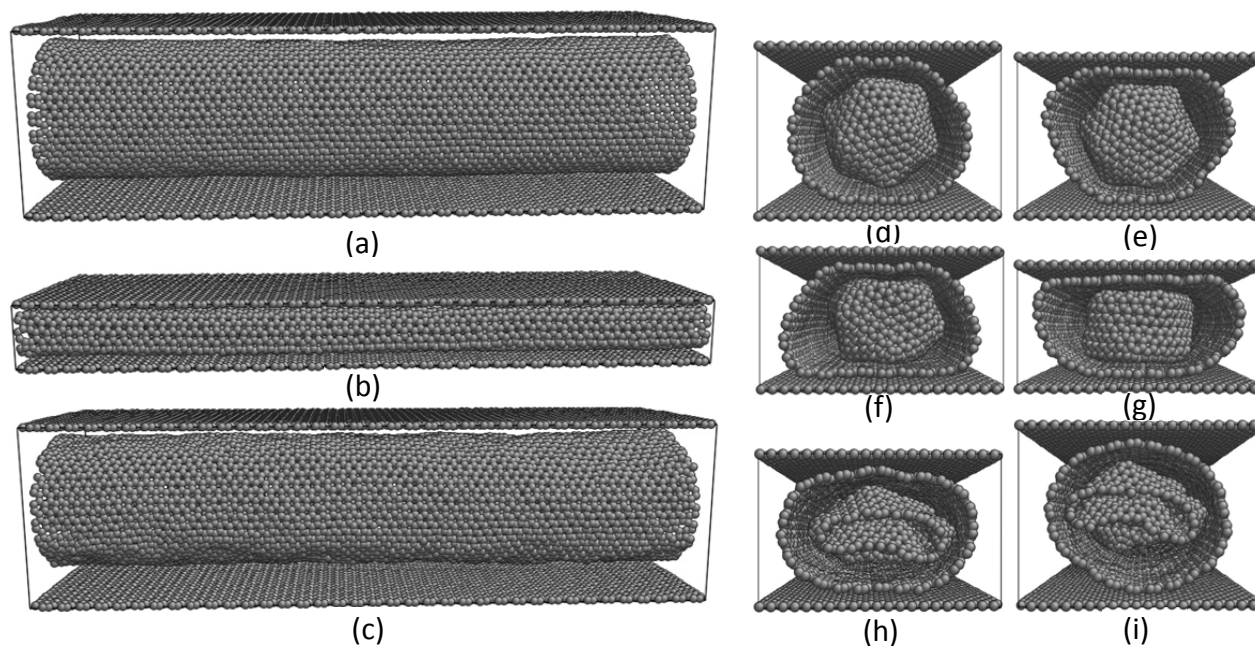


**Figure 2** Deformation evolution of the SWCNT with impact energy **4.152 keV**. (a) The initial configuration of the SWCNT. (b) Its maximum deformation. (c) The final status after detachment between the impactor and the EAS. (d) – (g) A loop of the trapezoid-shape deformation of the SWCNT during the process of (a) to (b) from the side view. (h) - (i) The deformation of buckyballs when the detachment happens.

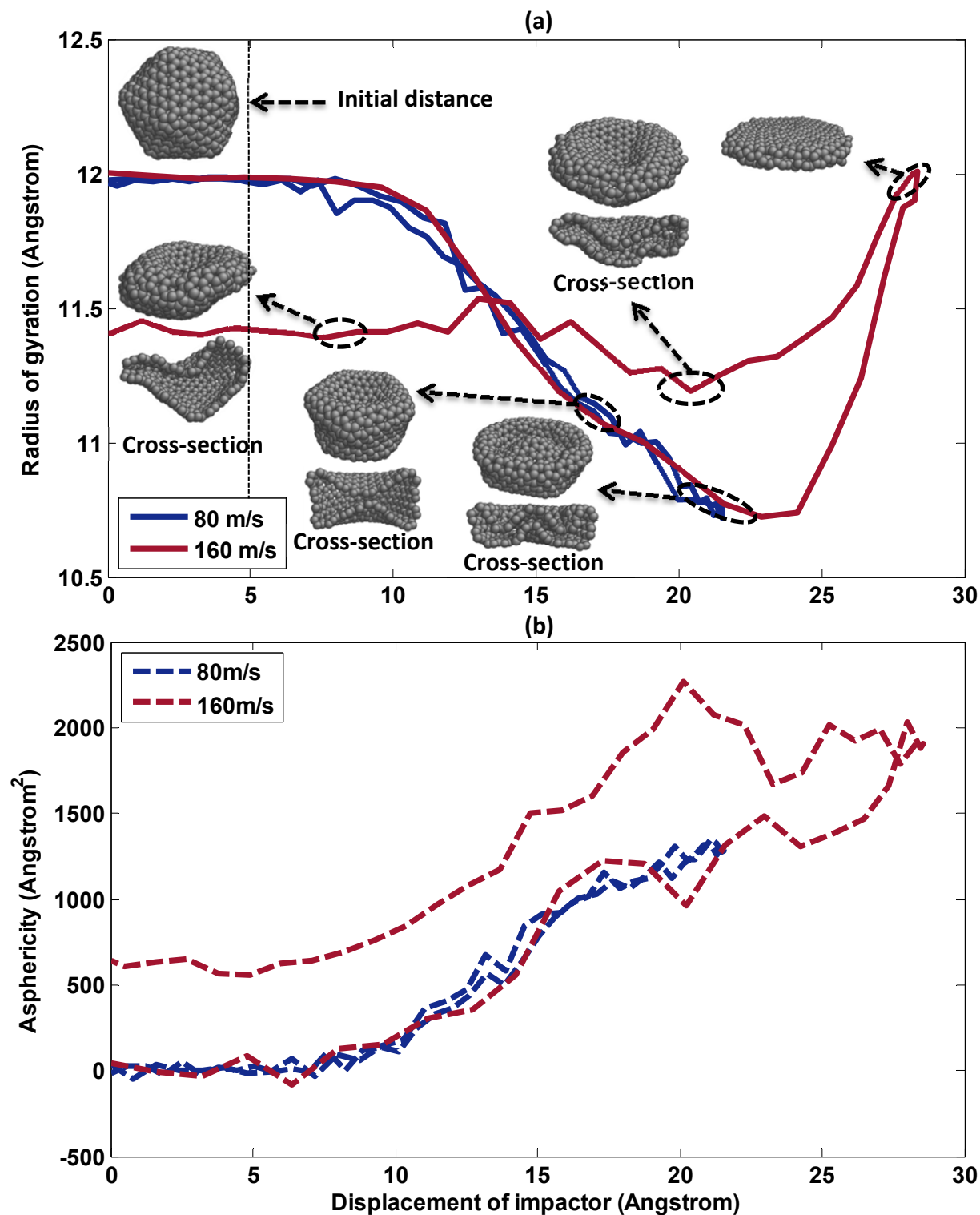


**Figure 3:** (a) RoG and (b) asphericity of buckyballs as a function of impactor displacement. Subplots show the deformation evolutions of a  $C_{720}$  buckyball during the impact process with

velocity **80 m/s** and **160 m/s** (impact energy **1.038 keV** and **4.152 keV**) respectively.

Morphologies of the buckyball in the dashed ellipse (the blue line and the red line) are similar.

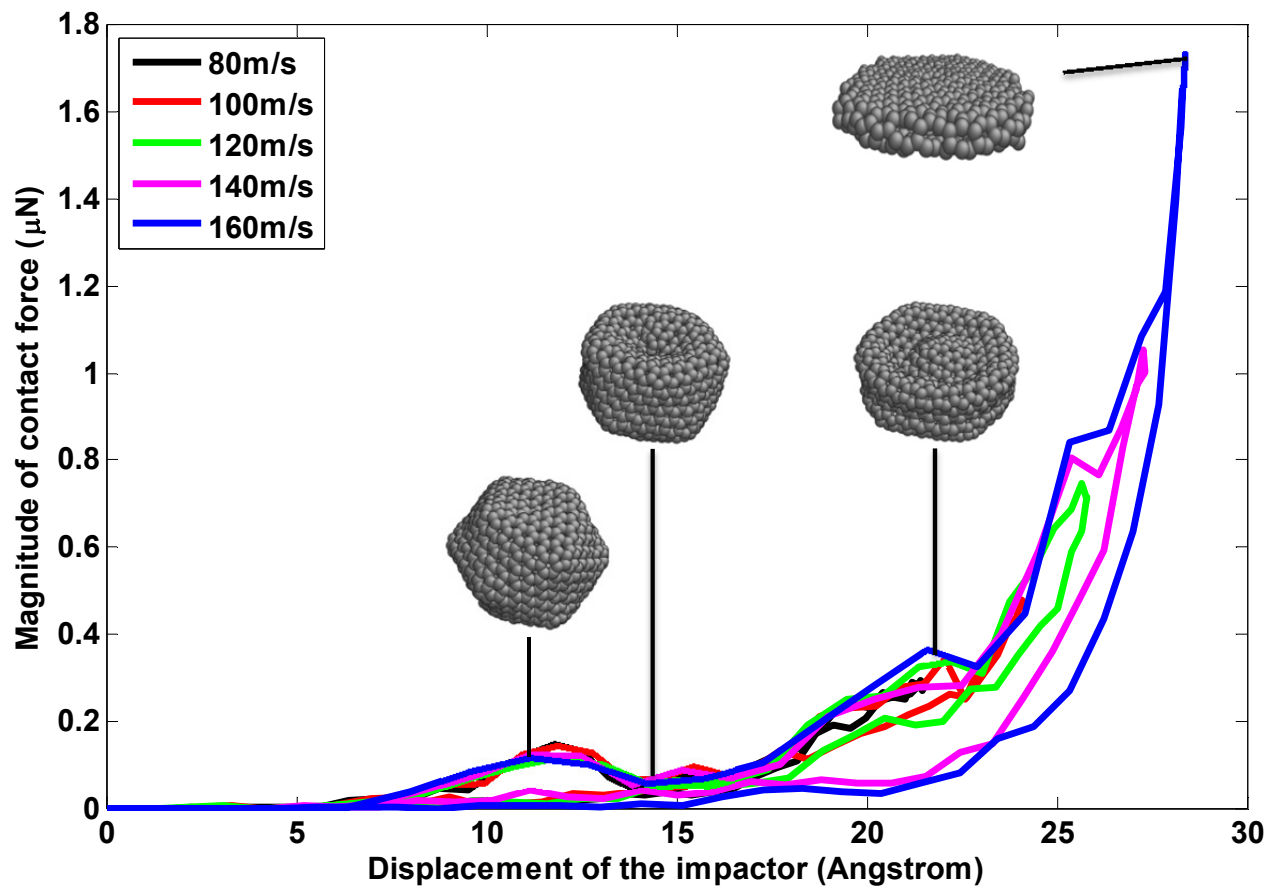


**Figure 4:** Contact force as a function of impactor displacement during the impact process with various impact energies as velocity increases from **80 m/s** to **160 m/s**.

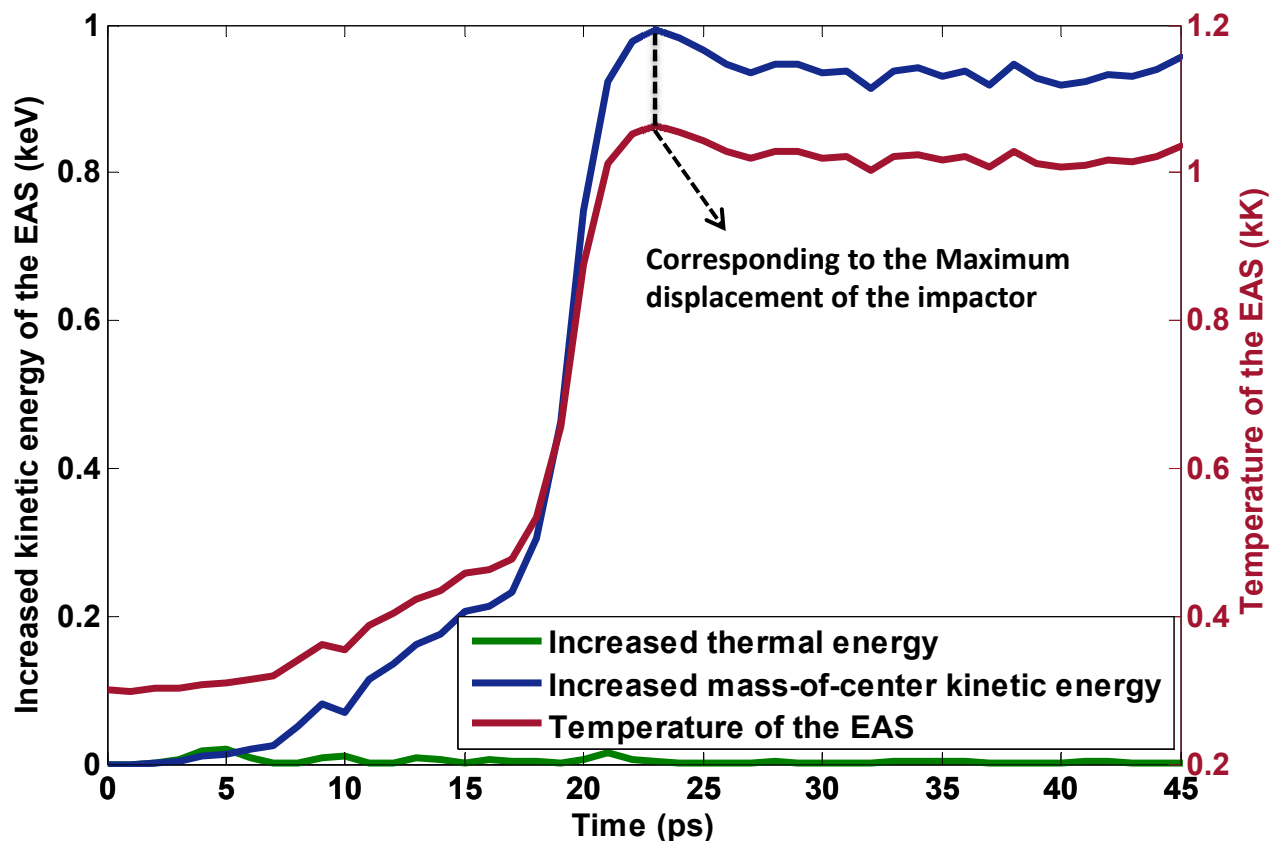


**Figure 5:** Increased thermal energy and center-of-mass kinetic energy as well as the temperature of the EAS under impact energy **4.152 keV**, as a function of time.

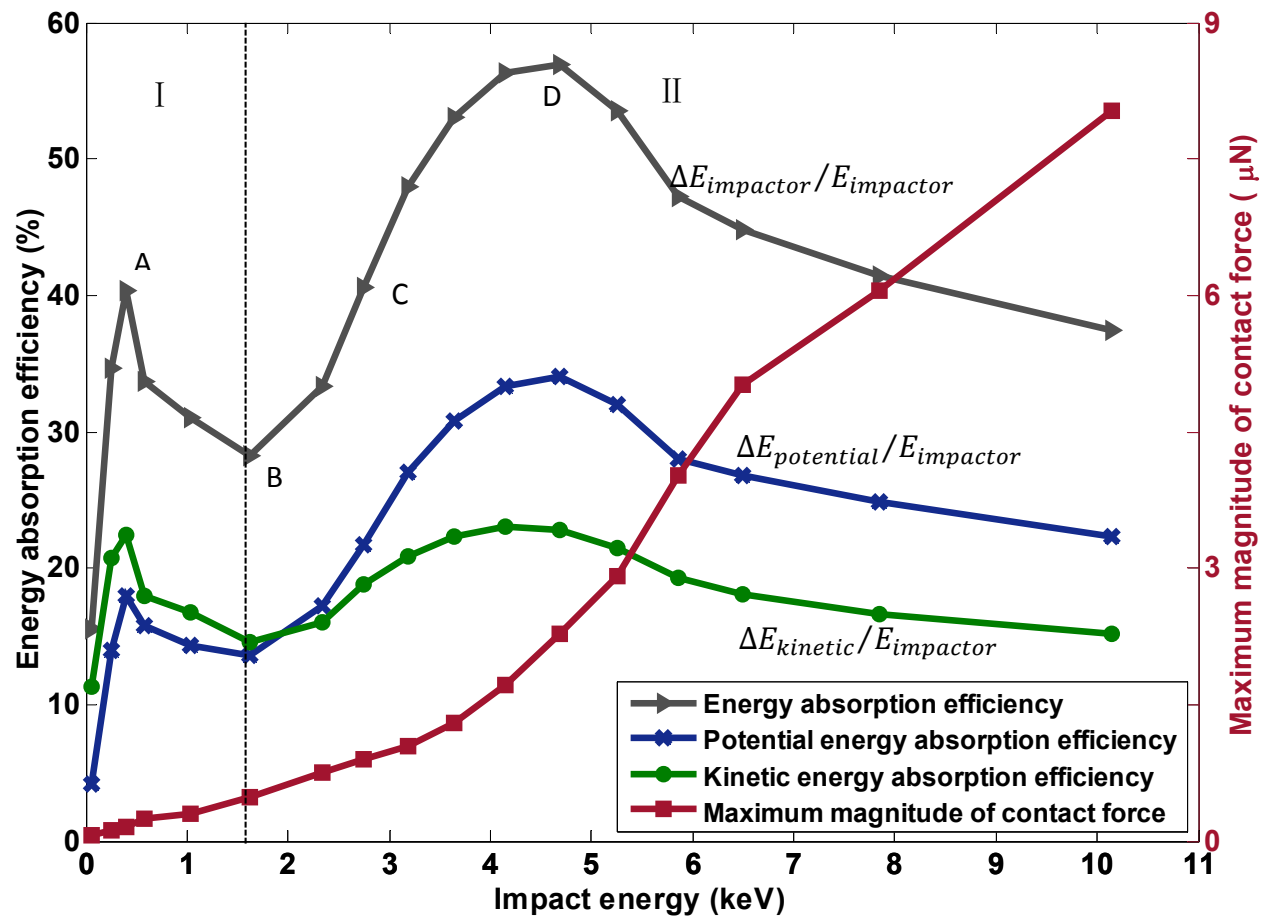


**Figure 6:** Energy absorption rate and maximum contact force upon impact with various impact energies (from  $6.488 \times 10^{-2}$  keV to 10.138 keV).

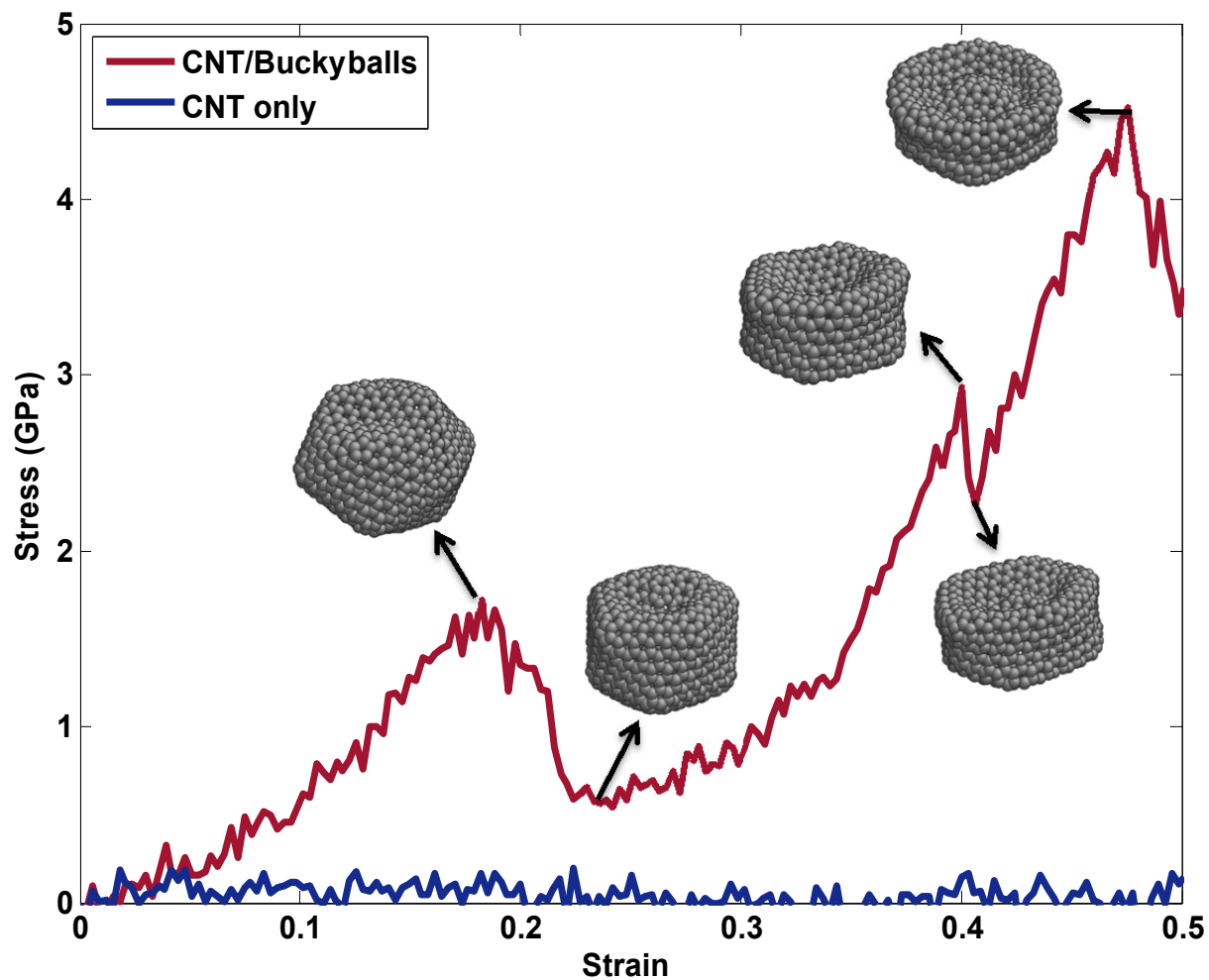
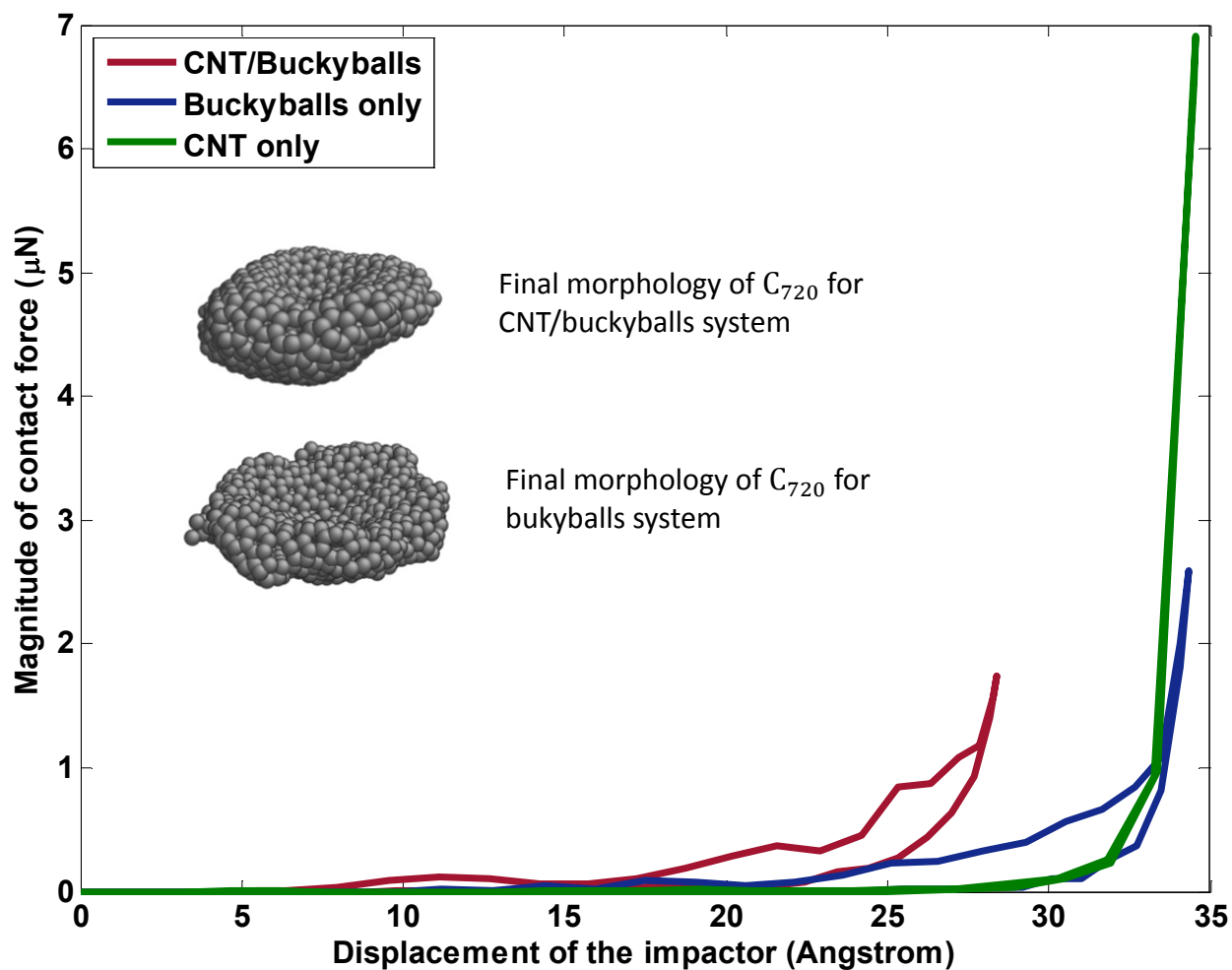
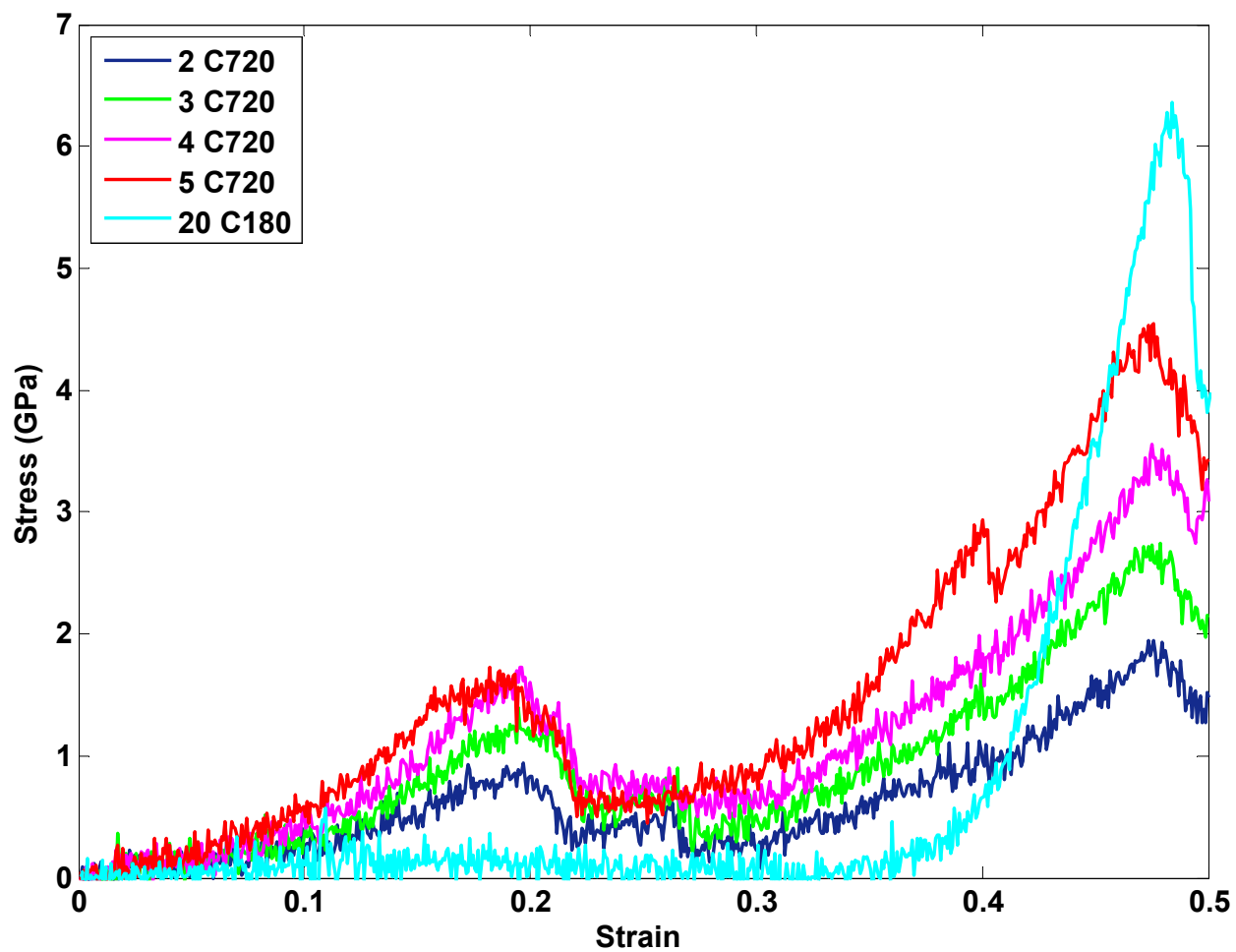


Figure 7: Stress-strain curves for both CNT/Buckyballs and CNT only systems under lateral compression



**Figure 8:** Contact force-displacement relationship during the loading and unloading process of the impact



**Figure 9:** Stress-strain curves for 2-C<sub>720</sub>, 3-C<sub>720</sub>, 4-C<sub>720</sub>, 5-C<sub>720</sub> EASes and 20-C<sub>180</sub> EAS under lateral compression

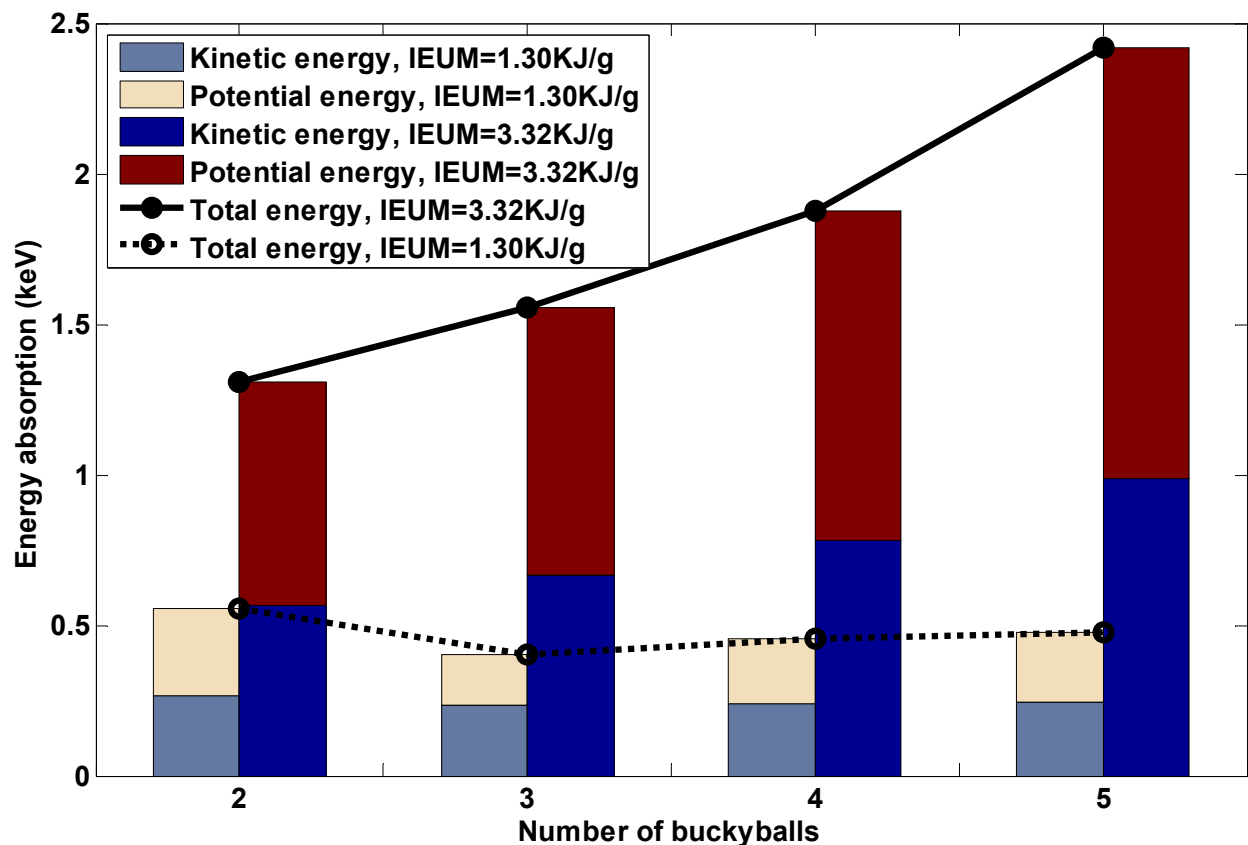


**Figure 10:** Energy absorption (including potential energy and kinetic energy) of 2-C<sub>720</sub>, 3-C<sub>720</sub>, 4-C<sub>720</sub> and 5-C<sub>720</sub> EASs with IEUM = 3.32 kJ/g and 3.32 kJ/g respectively.

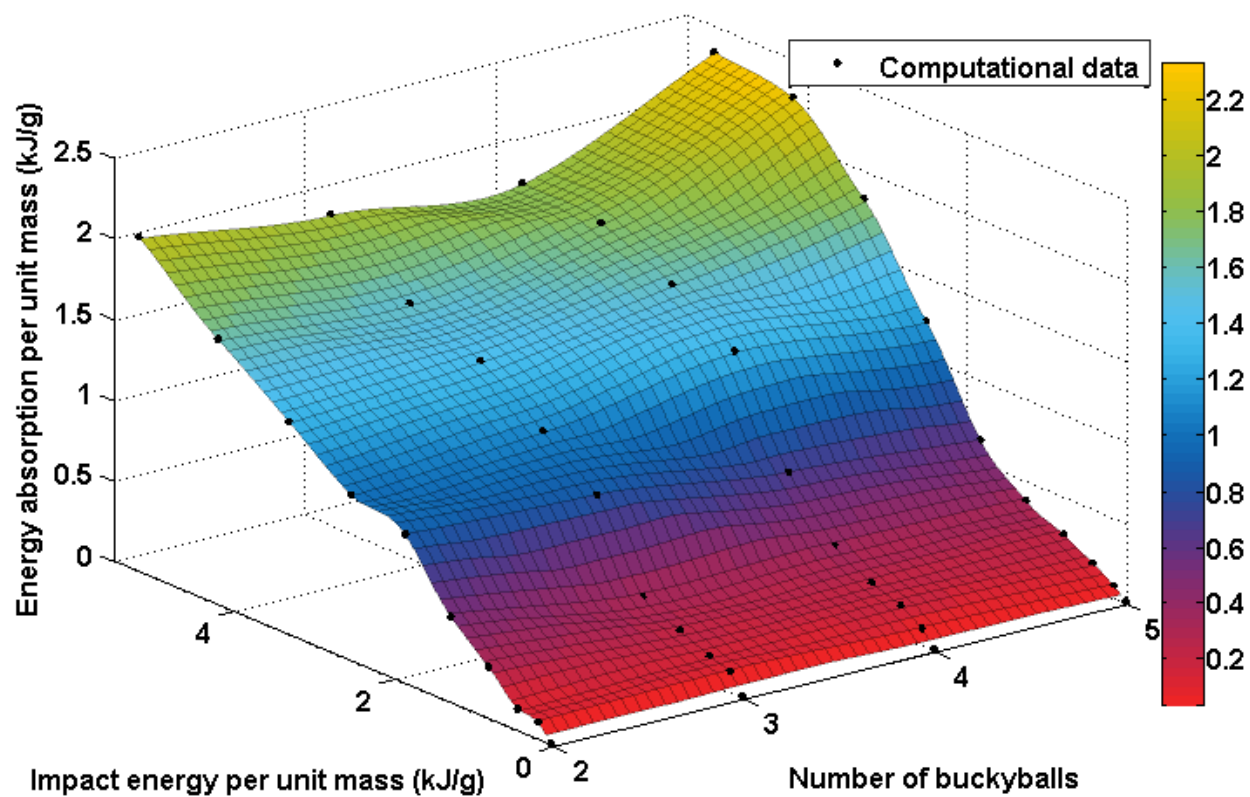


**Figure 11:** A fitting surface of EAUM of  $C_{720}$  EAS as a function of number of buckyballs and IEUM based on cubic spline interpolation. Number of buckyballs varies from 2 to 5 and IEUM varies from **0.05 kJ/g** to **5.19 kJ/g**.

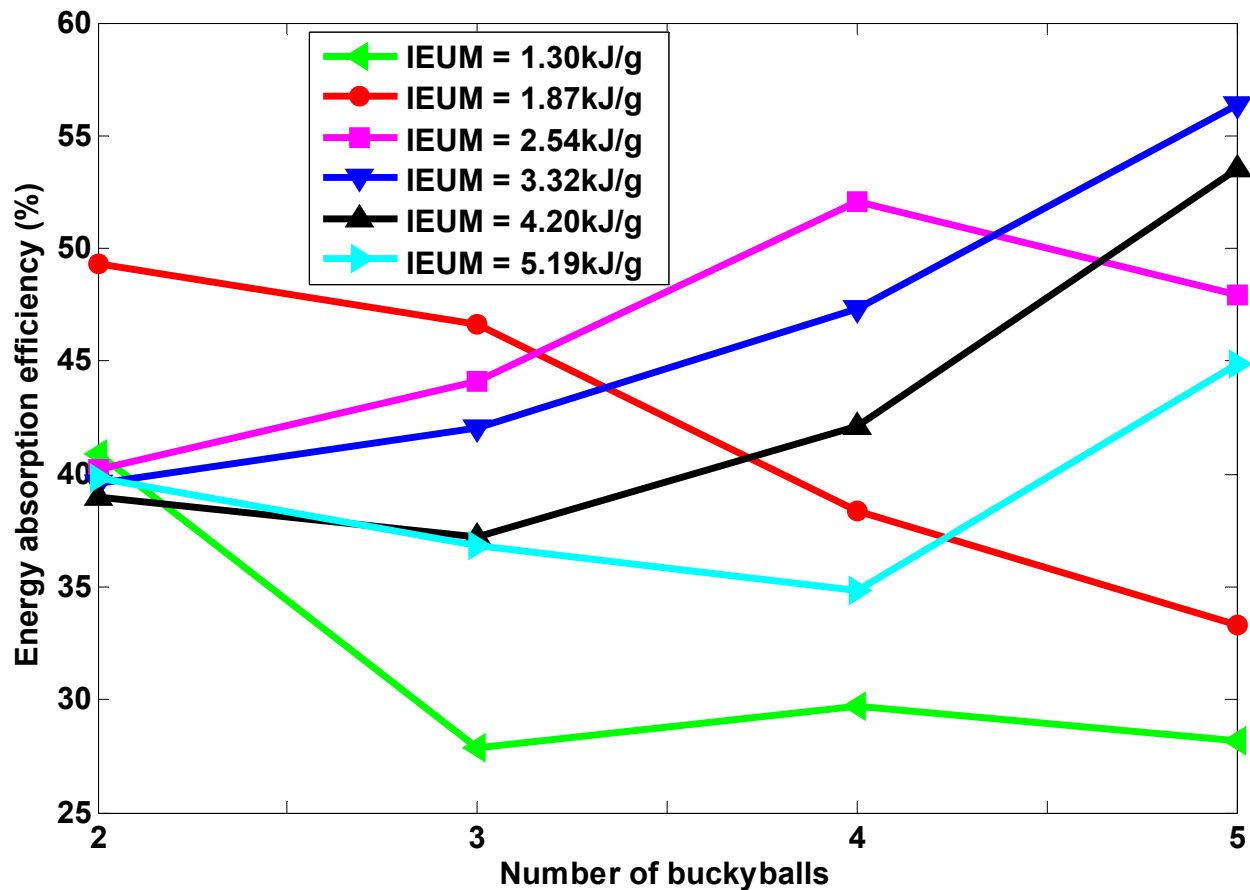


**Figure 12:** Energy absorption percentage of  $C_{720}$  EAS as a function of number of buckyballs, based on a series of IEUMs (varying from 1.30 kJ/g to 5.09 kJ/g).

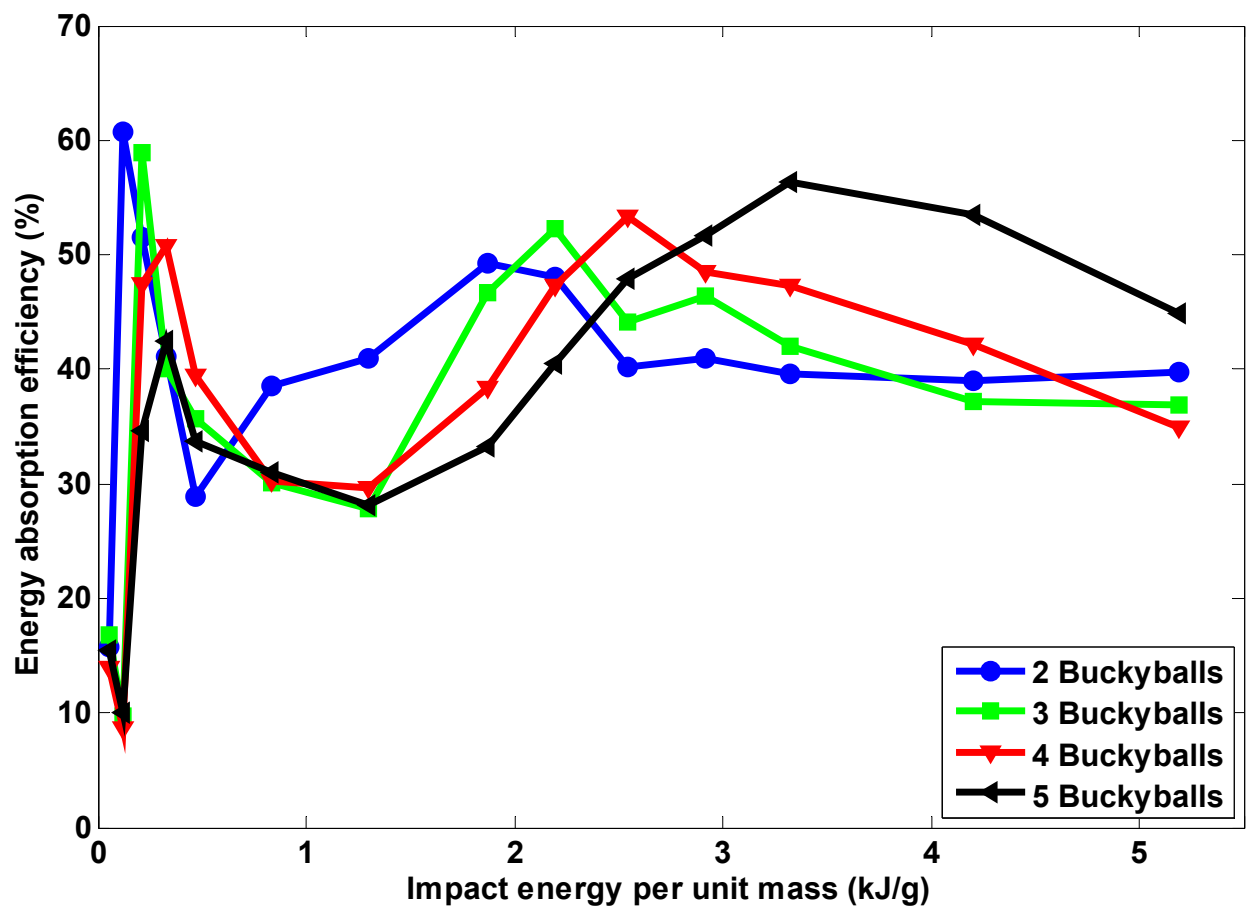


**Figure 13** Energy absorption percentage of 2- $C_{720}$ , 3- $C_{720}$ , 4- $C_{720}$  and 5- $C_{720}$  EASs respectively as a function of IEUM (varying from 0.05 KJ/g to 5.09 KJ/g).

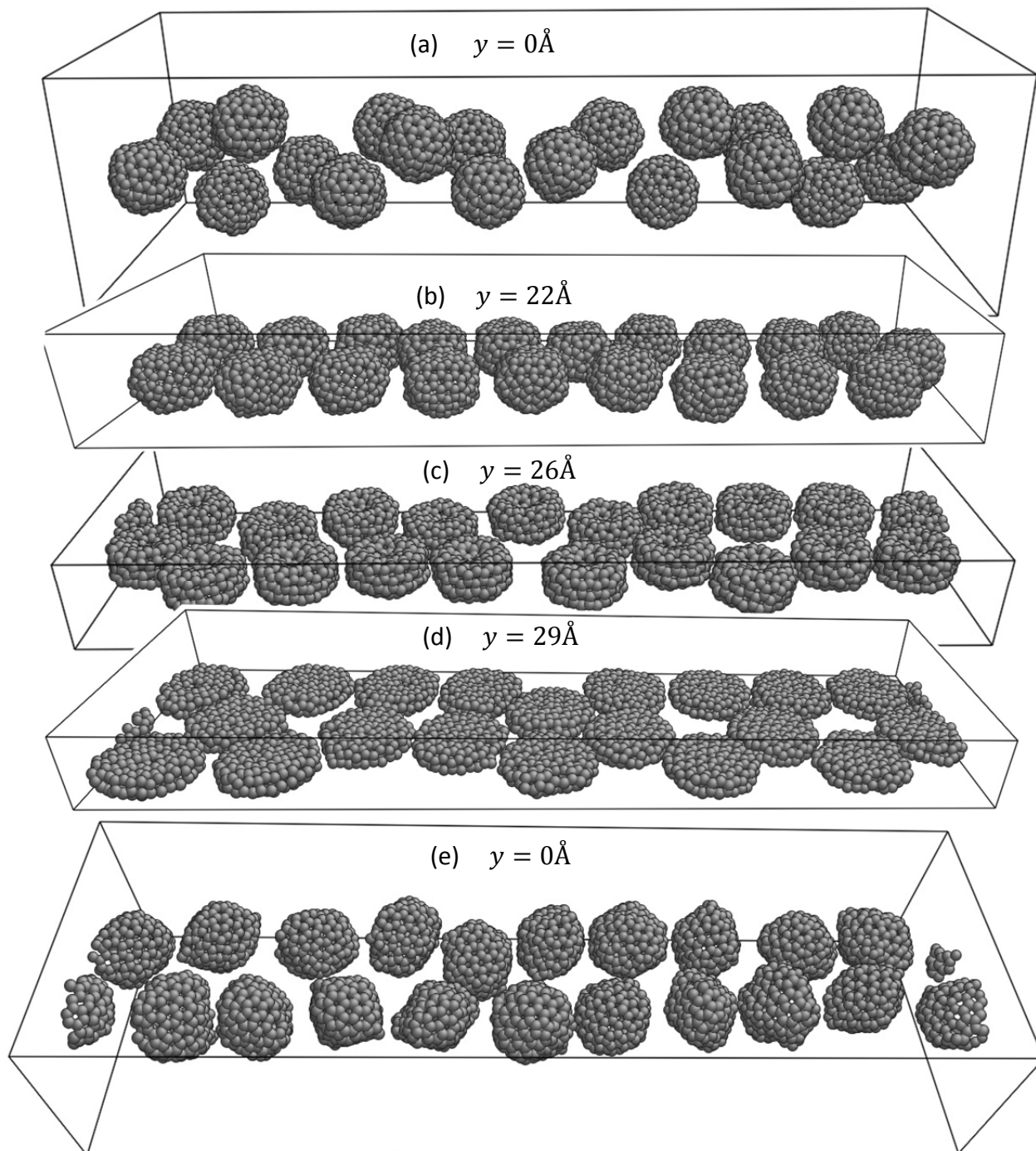


**Figure 14:** Deformation evolutions of  $\text{C}_{180}$  buckyballs of a 20- $\text{C}_{180}$  EAS with impact velocity 160 m/s.

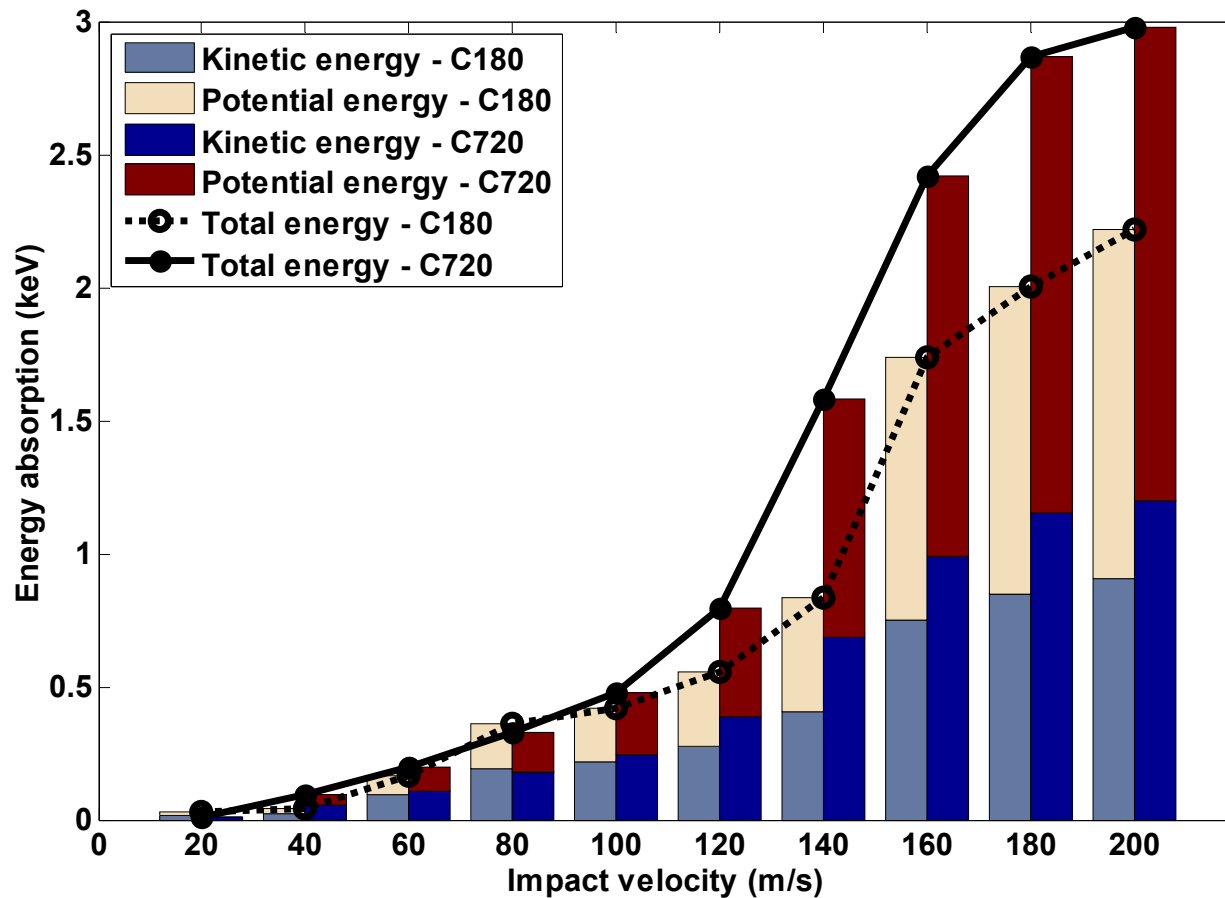


**Figure 15:** Energy absorption of the 5-C<sub>720</sub> EAS and 20-C<sub>180</sub> EAS upon impact with constant impact mass but various impact velocities.

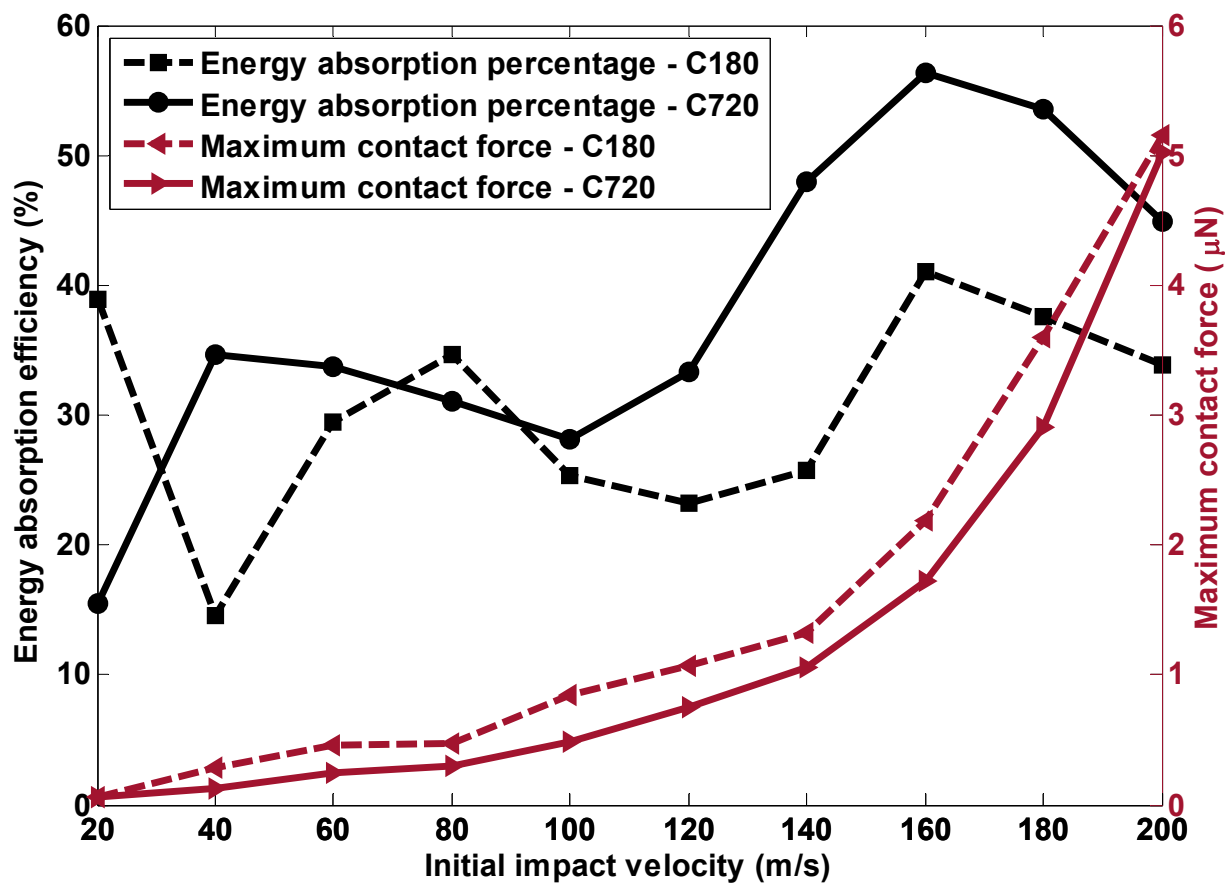


**Figure 16:** Energy absorption percentage and maximum contact force of the 20-C<sub>180</sub> EAS and 5-C<sub>720</sub> EAS as a function of initial impact velocity.